# SUPPLEMENTARY FIGURES

## Evolution, structure and function of the putative biosynthetic gene cluster of the fungal secondary metabolite myriocin, a potent inhibitory sphingolipid

Ben Rutter[1], Michael A Herrera[2], Gustavo Perez Ortiz[2], Claudio Greco[3], Ben Ashley[2], Hai Deng[4], Abigail Hay[1], Cameron Bedford[5], Marius Wenzel[6,7], Stephen Mondo[8], Zachary Konkel[9], Jason C Slot[9], Qinxi Ma[5], Nicolas Helmstetter[5], Rhys A. Farrer[5], Dominic J. Campopiano*[2] & Alexandra C Brand*‡[1,5,10]

[1] School of Medicine, Medical Sciences & Nutrition, University of Aberdeen, Aberdeen, UK

[2] School of Chemistry, University of Edinburgh, Edinburgh, UK

[3] Department of Biosciences, Swansea University, Swansea, UK

[4] Department of Chemistry, School of Natural & Computing Sciences, University of Aberdeen, Aberdeen, UK

[5] Medical Research Council Centre for Medical Mycology at the University of Exeter, Exeter, UK

[6] Centre for Genome-Enabled Biology & Medicine, University of Aberdeen, Aberdeen, UK

[7]School of Biological Sciences, University of Aberdeen, Aberdeen, UK

[8]US Department of Energy Joint Genome Institute, Lawrence Berkeley National Laboratory, Berkeley,, CA 94720, USA.

[9]Department of Plant Pathology, The Ohio State University, Columbus, USA

[10]Living Systems Institute, University of Exeter, Exeter, UK

*Co-senior authors

‡Corresponding author: Alexandra Brand a.brand@exeter.ac.uk

a ***I. sinclairii – Day 7***

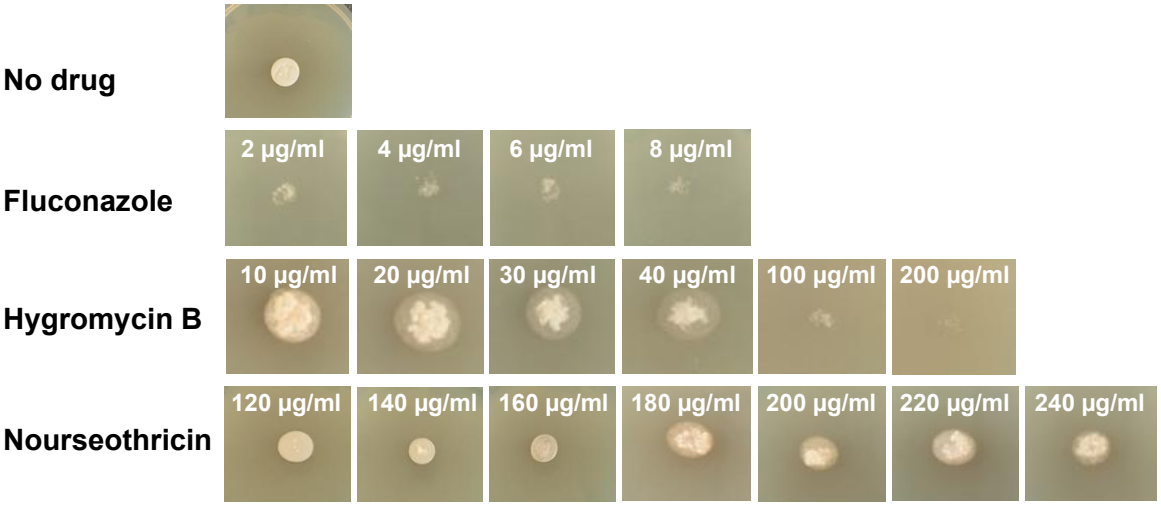


b ***M. sterilia – Day 5***

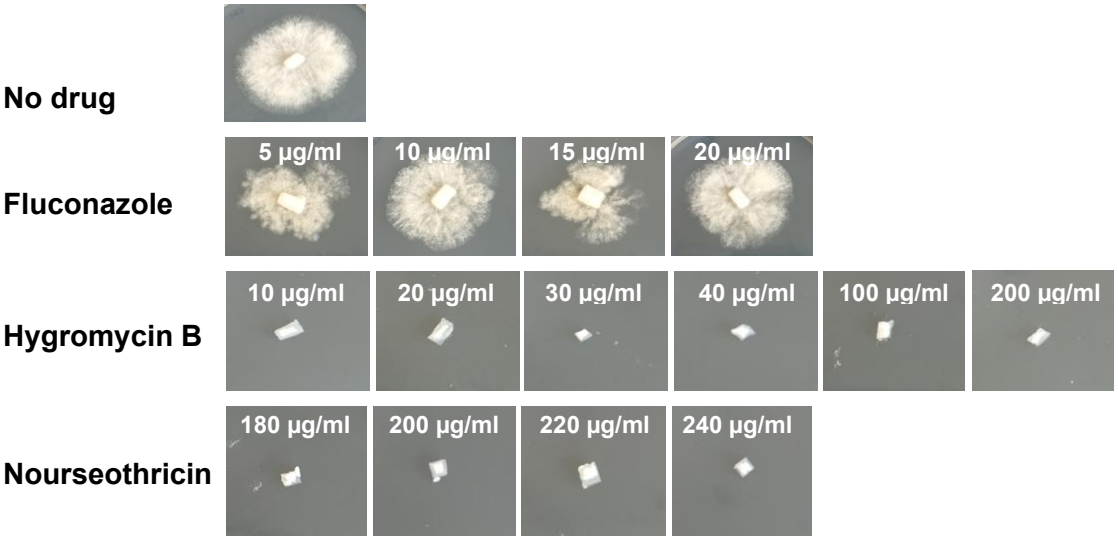


c

| Drug | *I. sinclairii* sensitivity (µg/ml) | *M. sterilia* sensitivity (µg/ml) |
|---|---|---|
| Fluconazole | < 2 | > 20 |
| Hygromycin B | 20 | < 10 |
| Nourseothricin | 240 | < 180 |

**Fig. S1: Susceptibility of *I. sinclairii* and *M. sterilia* to fluconazole, hygromycin B and noursethricin.** *I. sinclairii* or *M. sterilia* were inoculated onto tryptic soy agar or potato dextrose agar, respectively, containing increasing concentrations of the antifungal agents fluconazole, hygromycin B or nourseothricin. A) *I. sinclairii* plates were incubated at 25 °C for 7 d. B) *M. sterilia* plates were incubated at 37 °C for 5 d. C) Sensitivity was quantified by measuring the ratio of colony diameter compared to the no-drug control.

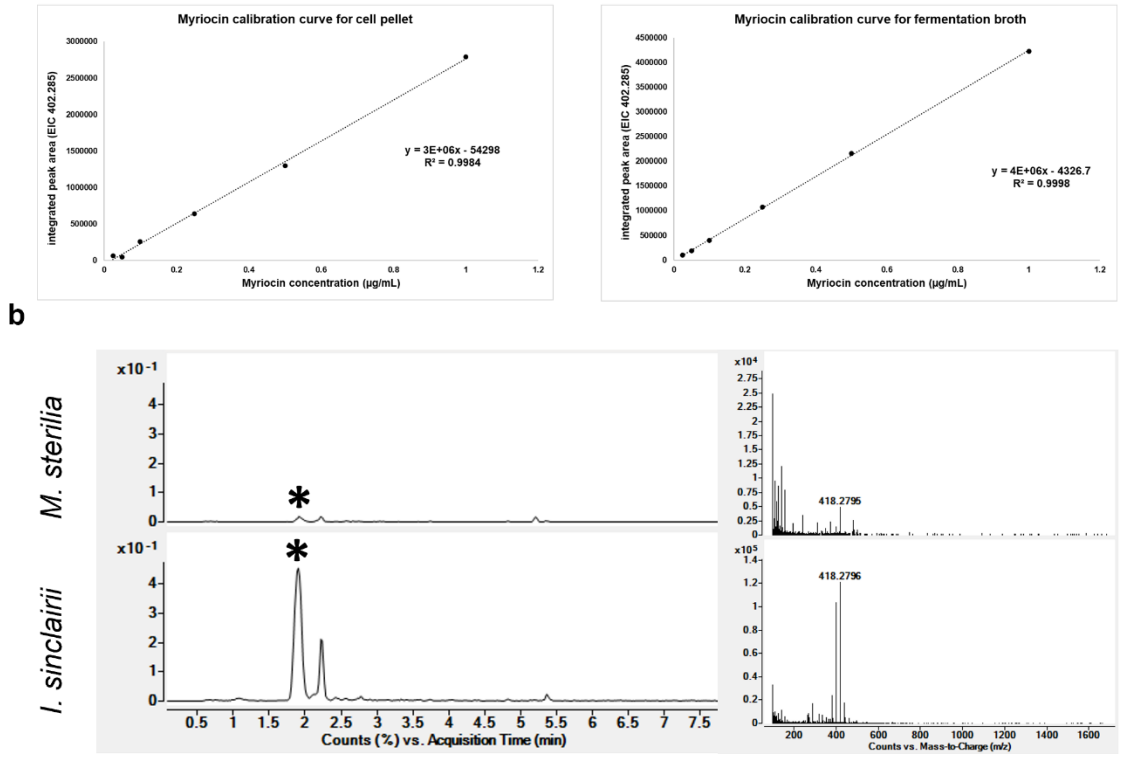


**Fig. S2: Myriocin quantification and detection of myriocin derivates.** a. Calibration curves for the quantification of myriocin for the cell pellet (left) and for the fermentation broths (right). b. UHPLC-HRMS analysis in positive mode of the organic extracts for the myriocin derivative. EIC for 418.28, noted with an * (left) and mass spectra (right) for *M. sterilia* (top) and *I. sinclairii* (bottom).

a

| Assembly parameters | *I. sinclairii* | *M. sterilia* |
|---|---|---|
| Total genome size (bp) | 25,179,760 | 34,156,770 |
| Number of contigs | 59 | 141 |
| Maximum contig length (bp) | 2,840,681 | 2,447,423 |
| Mean Illumina coverage | 222 | 139 |
| Mean MinION coverage | 42 | 61 |
| BUSCO completeness (%) | 98.6 | 99.3 |
| N50 value (bp) | 1,423,211 | 817,506 |
| Properly paired (%) | 99.63 | 98.29 |
| GC (%) | 57 | 56 |
| Total number of non-ATGC characters | 0 | 0 |
| Total number of proteins/genes | 8167 | 8706 |
| Secondary metabolite clusters (AntiSMASH) | 27 | 20 |

b *I. sinclairii*

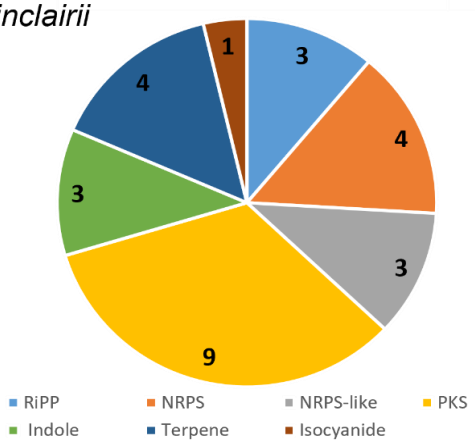


| Secondary Metabolite Class | Amount |
|---|---|
| RiPP | 3 |
| NRPS | 4 |
| NRPS-like | 3 |
| PKS | 9 |
| Hybrid PKS - NRPS | 0 |
| Indole | 3 |
| Terpene | 4 |
| Isocyanide | 1 |
| **Total** | **27** |

c *M. sterilia*

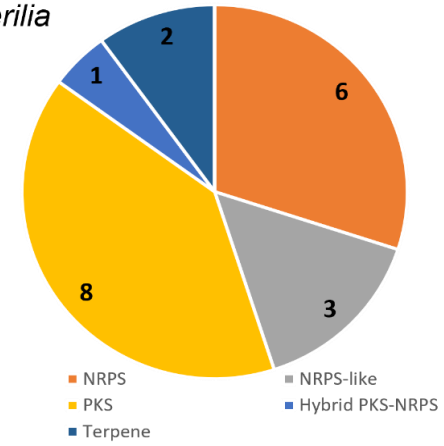


| Secondary Metabolite Class | Amount |
|---|---|
| RiPP | 0 |
| NRPS | 6 |
| NRPS-like | 3 |
| PKS | 8 |
| Hybrid PKS-NRPS | 1 |
| Indole | 0 |
| Terpene | 2 |
| Isocyanide | 0 |
| **Total** | **20** |

**Fig. S3: Genome assembly parameters and antiSMASH analysis of secondary metabolite gene clusters by class.** a. Comparison of genome assembly parameters for *I. sinclairii* and *M. sterilia*. b,c. Breakdown of secondary metabolite biosynthesis gene clusters by class (AntiSMASH V7.1.0). Putative classifications are based on antiSMASH v7.1.0 fungal mode; RiPP and indole predictions may include false positives and require experimental validation (e.g., via precursor peptide identification or metabolomics). No RiPP BGCs were linked to characterized metabolites in these genomes.

a

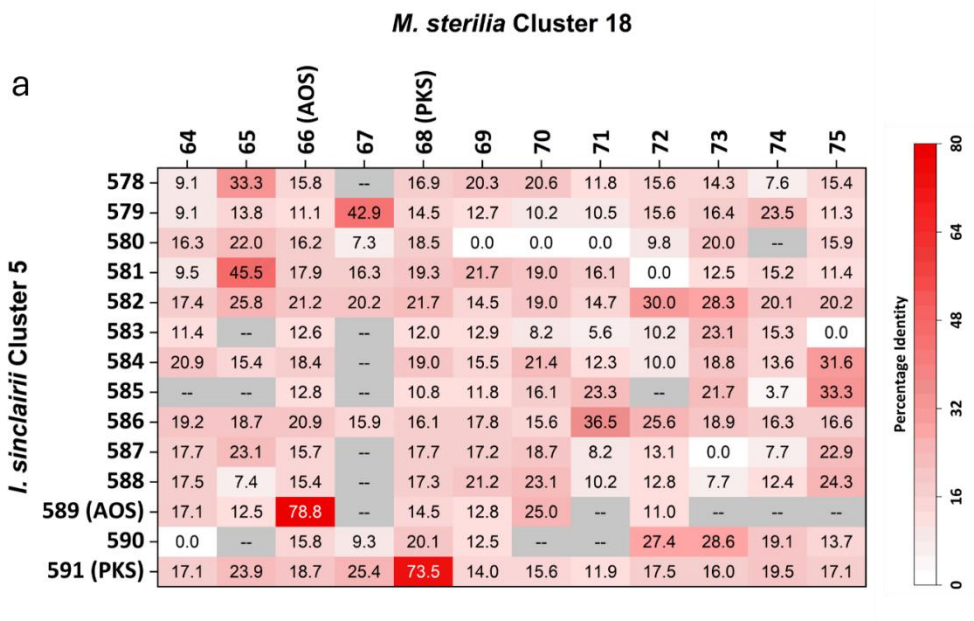


b

| Primer name | Primer sequence (5′ – 3′) | Product size (bp) |
|---|---|---|
| MsmyrA_1-F | GGCTGGTGAAGCACTTCTT | 186 |
| MsmyrA_1-R | CCAGCTGCAGGTGGAAGAC | |
| MsmyrB_1-F | GCTCGCATGATCGACAACTA | 201 |
| MsmyrB_1-R | CGTGAACACCATCACGACGTT | |
| MsActin-F | CCAACATAGTCCTCTCAGGC | 164 |
| MsActin-R | TGAGACCGGCAAGAATACTG | |
| IsmyrA_1-F | CCATCGACTTCTGCTCCAAC | 181 |
| IsmyrA_1-R | CCGTGAAAGTCGGCAATCTC | |
| IsmyrB_1-F | CGCTCATCAAGATGGTCATG | 169 |
| IsmyrB_1-R | CCAAACGAGTTGAGGCTGAT | |
| IsActin-F | AATCAACCCCAAGTCCAACC | 169 |
| IsActin-R | AAATGGGAACAACGTGGGTG | |

**Fig. S4:** a. Identification in *I. sinclairii* and *M. sterilia* genomes of a shared gene cluster revealed the predicted iPKS and AOS genes required for myriocin biosynthesis, which were expressed concomitantly with myriocin biosynthesis. A heatmap indicates the percentage identities for each pair of open reading frames (ORFs) within the two clusters in *M.sterilia* (Cluster 18) and *I. sinclairii* (Cluster 5); b. Primers derived from the above clusters and used for RT-PCR of *myrA*, *myrB* and actin (internal control) mRNA isolated from *I. sinclairii* and *M. sterilia*.

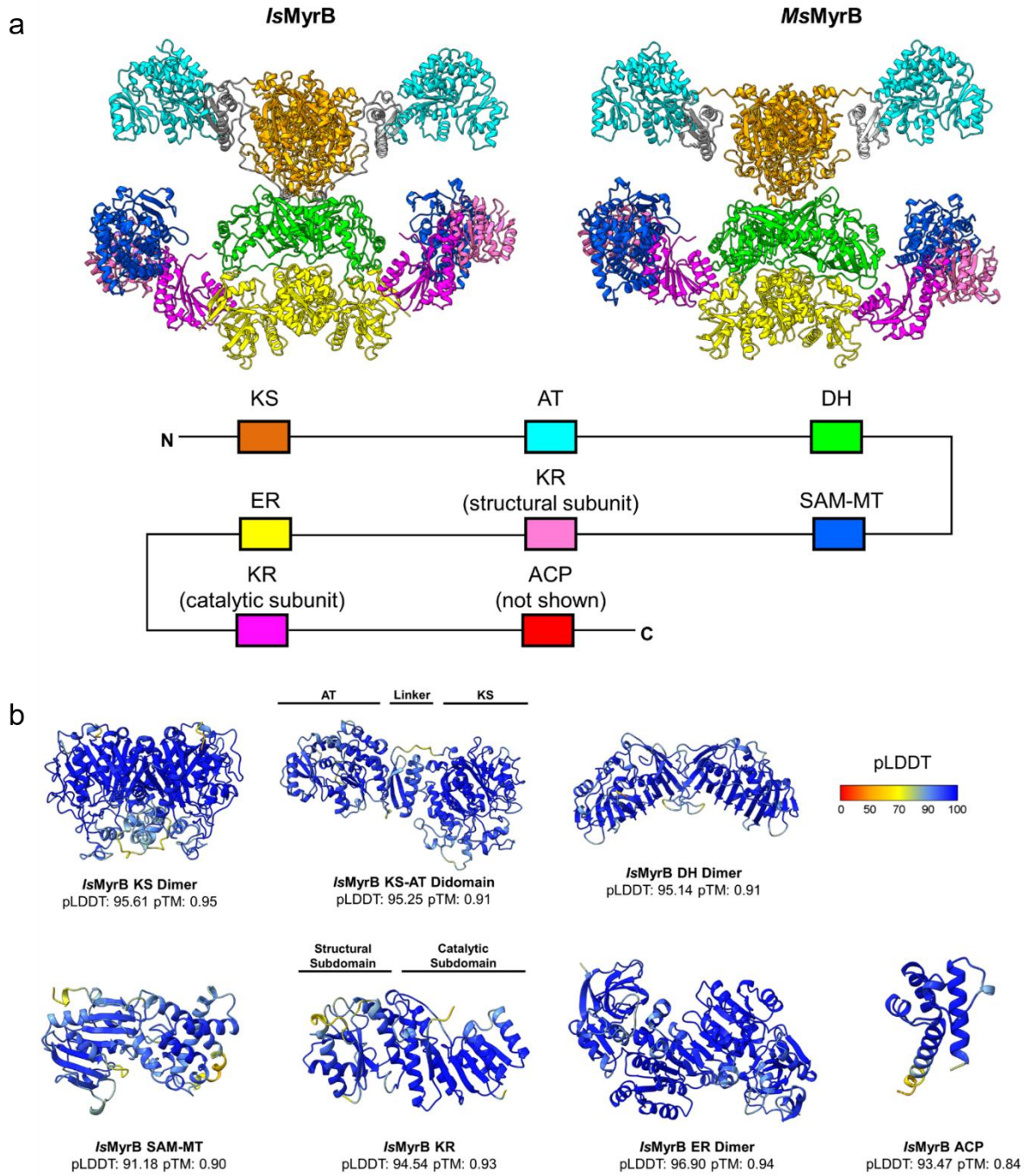


**Fig. S5: a. Composite predicted structural models showing the relative domain organisation of the IsMyrB and MsMyrB homodimers.** Mammalian fatty acid synthase (PDB: 2VZ8) was used as a template guide, using structural alignment tools in PyMOL. Acyl Carrier Proteins (ACPs) have been omitted. Colours indicate active domains: KS = Ketoacyl Synthase, AT = acytransferase, DH = dehydratase, SAM-MT = *S*-adenosylmethionine-dependent methyltransferase. KR = ketoreductase, ER = enoylreductase. b. The constitutive domains of IsMyrB, coloured by pLDDT confidence score (0-100).

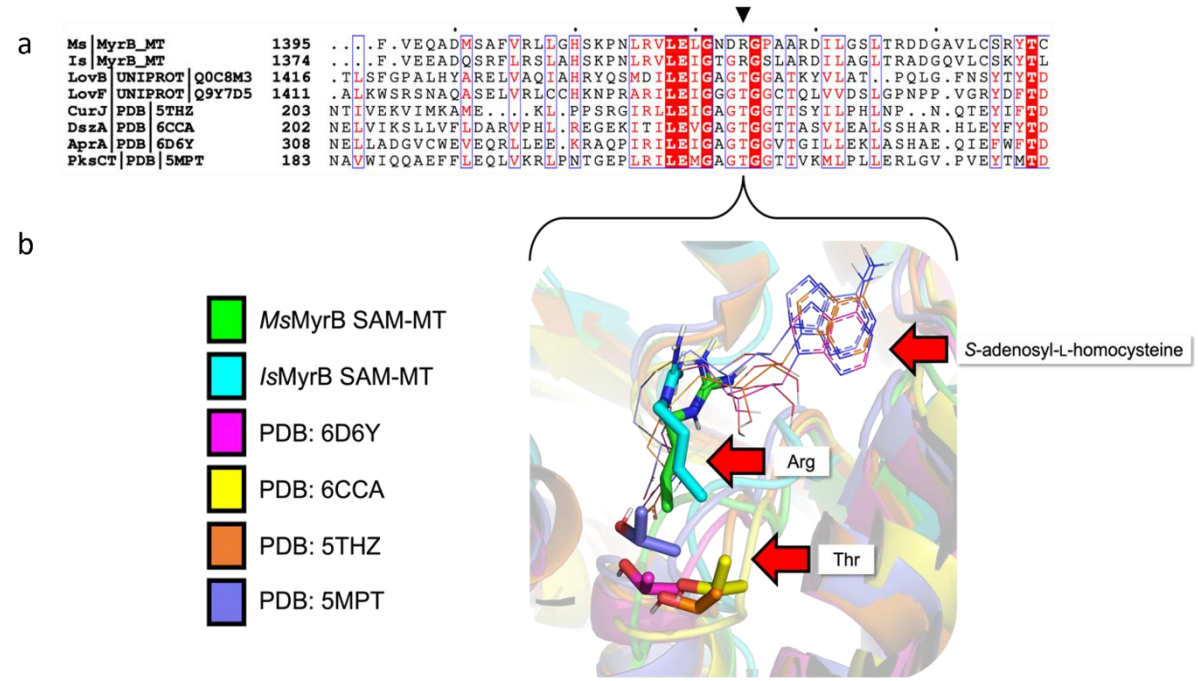


**Fig. S6: Occlusion of the *Is*MyrB and *Ms*MyrB *S*-adenosylmethionine binding pocket by a key threonine →arginine mutation.** a. Comparison with active, homologous S-adenosylmethionine methyltransferases (SAM-MTs) from the Protein Data Bank revealed a shared mutation in *I. sinclairii* and *M. sterilia* where the 3-carbon threonine is substituted by a 6-carbon arginine (black arrow). b. Modelling suggests that this substitution occludes the S-adenosylmethionine binding pocket, which likely inactivates the domain and correlates with the lack of methyl branching in myriocin. PDB = Protein Data Base.

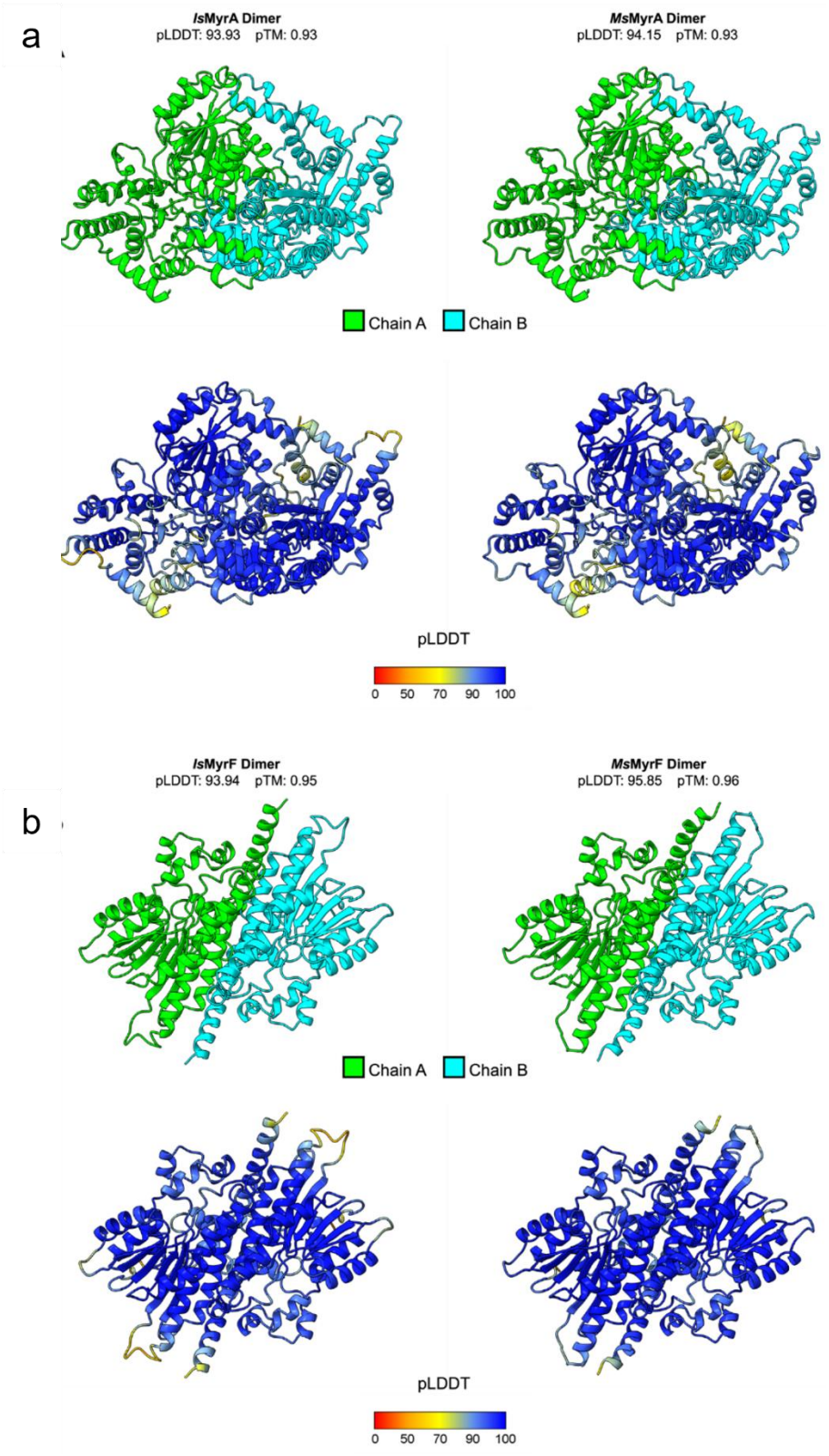


126

127 **Fig. S7: Structural models of MyrA (AOS) and MyrF (ketodihydrosphingosine reductase –**
128 **KDRS).** a. Structural models of IsMyrA and MsMyrA, coloured by chain (top) and pLDDT confidence
129 score (bottom, 0-100). b. Structural models of IsMyrF and MsMyrF, coloured by chain (top) and
130 pLDDT confidence score (bottom, 0-100).

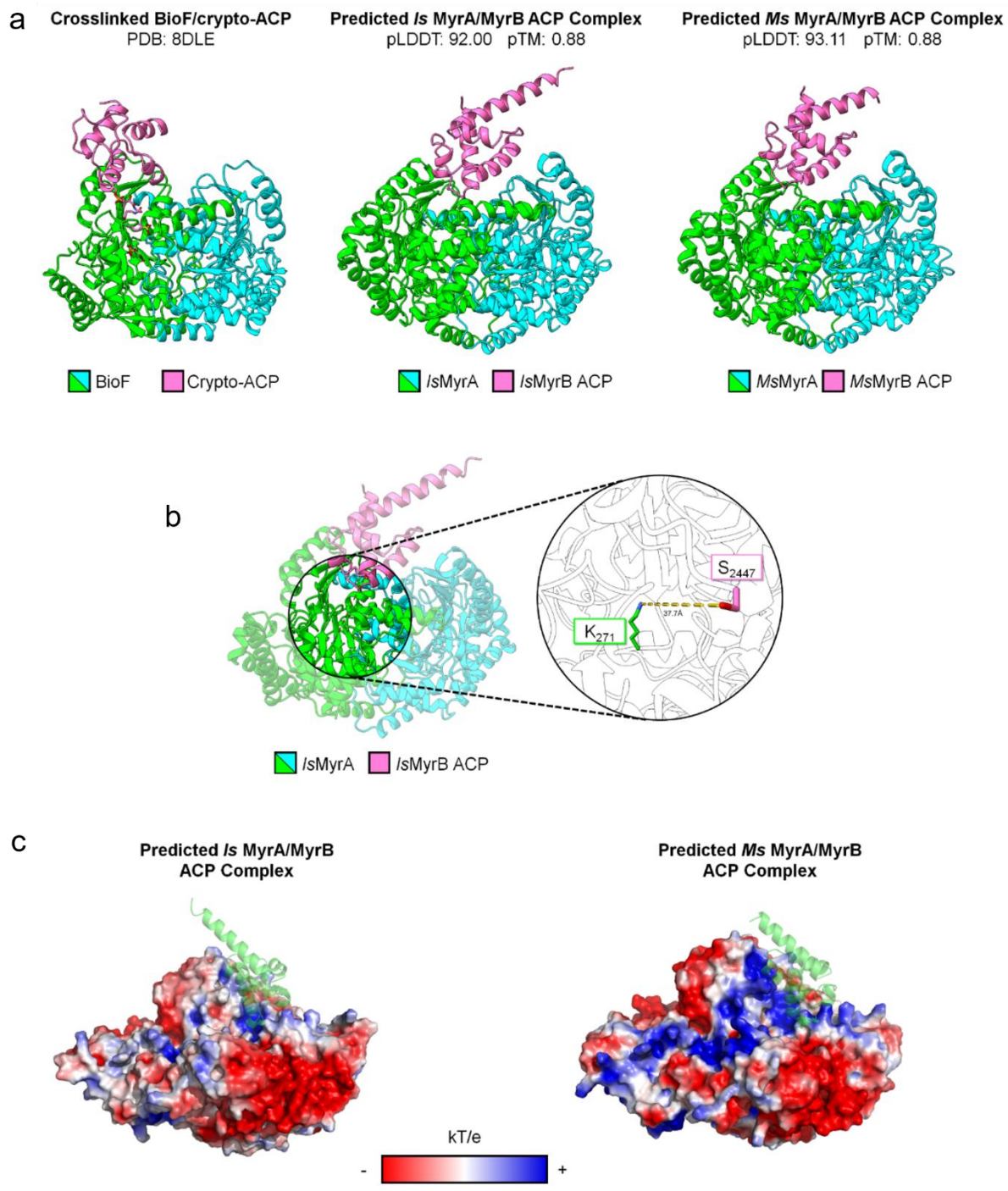


**Fig. S8: Interaction between the predicted MyrA (AOS) and MyrB (iPKS) acyl carrier protein complexes.** a. Comparison between *E. coli* BioWF/crypto-acyl carrier protein (ACP) experimental structure and the predicted MyrA and *Is*MyrB ACP complexes. b. Predicted docking interface between *Is*MyrA and *Is*MyrB ACP, showing the catalytic *Is*MyrB $S_{2447}$ positioned directly above the substrate binding tunnel of *Is*MyrA. c. Computed MyrA APBS electrostatic surface potentials, identifying patches of electropositivity around the AOS-ACP docking interface. MyrB ACPs are shown in green.

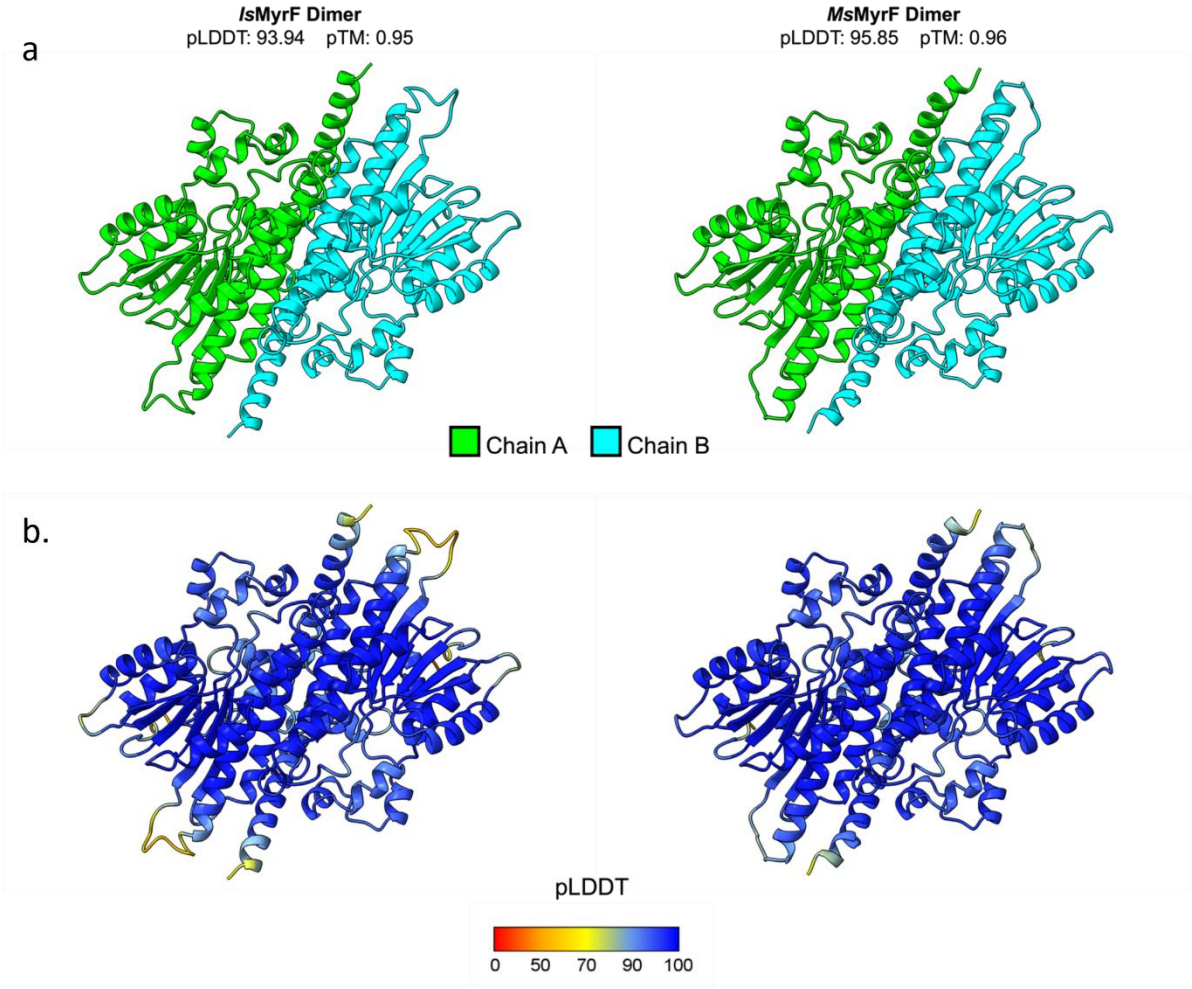


**Fig. S9: Structural models of *Is*MyrF and *Ms*MyrF homodimers.** a. Models coloured by chain. b. Models colours by pLDDT confidence score, as shown.

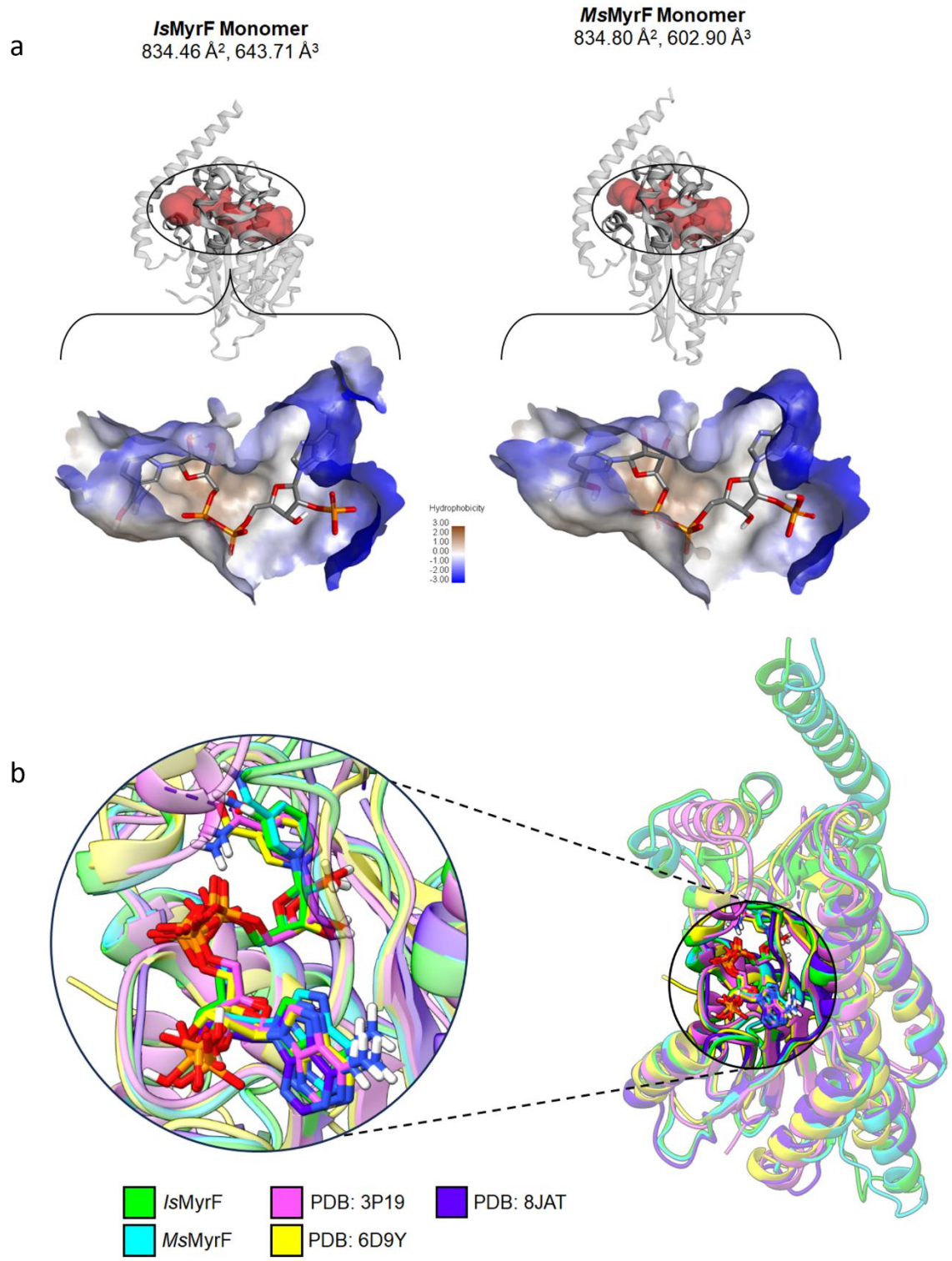


157

158

159

160 **Fig. S10: Structural analysis of *Is*MyrF and *Ms*MyrF (myriocin ketodihydrosphingosine**
161 **reductase (KDSR)).** a. Identification of a binding pocket in MyrF by topological analysis (CASTp3.0).
162 NADP+ was docked in the identified binding pockets (- 12.5 kcal $mol^{-1}$) and Kyte-Doolittle hydropathy
163 surfaces were visualised in BIOVIA Discovery Studio 2020. b. Superimposition of homologous,
164 NAD(P)-bound crystal structures over MyrF (with $NADP^+$ docked).

a

MAAASFLASWIRGQKLRAPQMKDAPTFFRNLEEALDVRRVDHAMFTRTKSTWKTGDAIDF
CSNDLLSLGSTGQLRAAFLDELAQNPGFALYAGGSRLMDGNYDYIEQVEQEIADFHGAET
ALIVASGYEGNAAIYSAIPRPGDAIVYDELVHASTHDGMAHSLALTRAAFRHNDVDSFRD
TLTSVVDSQPMIRDGSRTIIVSVESVYSMDGDVCPLVELLEVAREVCPKGNTAFVVDEAH
ATGILGPNGAGLVNALGVENDIAIRLHTCGKALASTGAVILGNATVRTALMNFARSVIYT
TAPSFPSVAGIRAAYNLMRTGATKKPQDNIQHLVKYFFKTISSNPIWEKANDMGILSIPV
SDDWESRDFVAHIVPVWTRQRYNWWLVFHLQLSGISAFPIDYPTVPKGQSRIRVMFHAAN
TEADADFLAATICNWAKEMIDIEEGAEGKGKMPKAAQQVYALMAANA*enlyfqg*HHHHHH

b

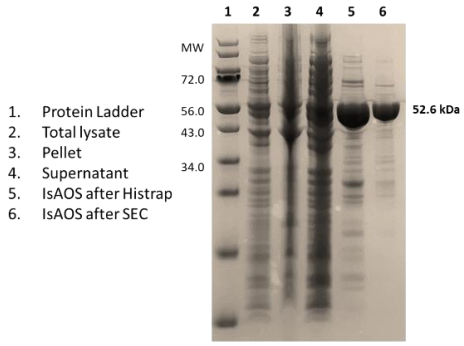


c

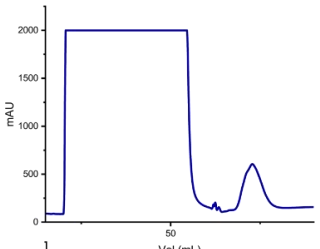


d

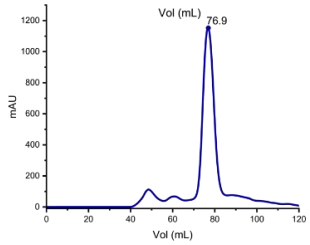


e

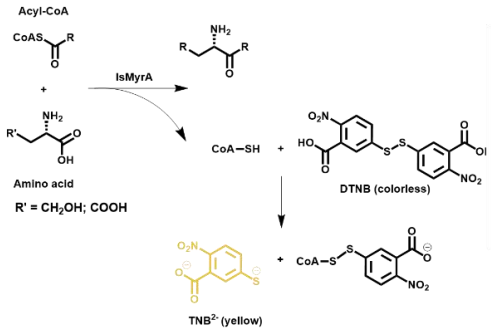


f

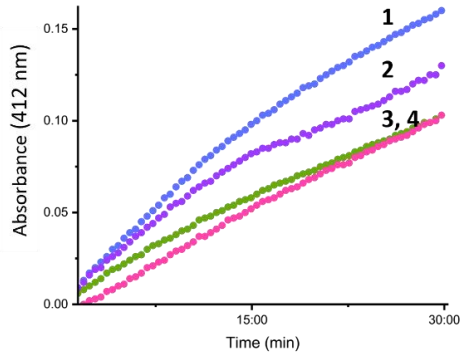


g

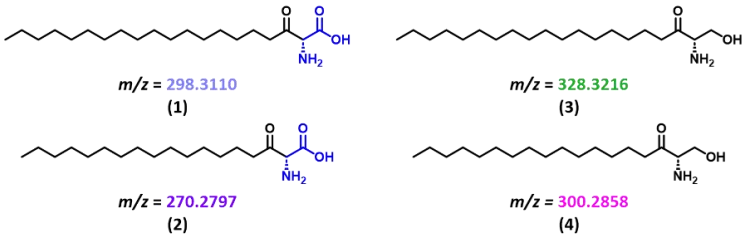


**Fig. S11: IsMyrA protein purification and DTNB activity assay.** a. Sequence of recombinant IsMyrA construct. b. SDS-PAGE gel of purification of IsMyrA. HiMark Pre-stained Protein Standard was used as ladder. Lanes 2 to 6 show each step of purification from transformed *E. coli* BL21 (DE3) 18+ hours post-induction using IPTG. See Fig. S14 for uncropped gel image. c. IsMyrA IMAC chromatogram. Cell-free extract was loaded using an AKTA start onto a 5 mL Nickel His-Trap FF column and eluted with a 10 – 300 mM imidazole gradient. Protein was detected at 280 nm. d. SEC purification of IsMyrA using a HiLoad 16/600 Superdex 200 pg (120 mL) SEC column, monitored at 280 nm. e. DTNB assay general reaction. The activity of IsMyrA was detected by capturing the CoASH released with 5,5′-dithiobis-(2-nitrobenzoic) acid (DTNB) and the spectrophotometric detection of the $TNB^{2-}$ anion (412 nm). f. IsMyrA activity against acyl-CoAs ($C_{16}$ and $C_{18}$) and amino acids aminomalonate and L-serine, detected using the DTNB assay. Raw data is available at https://doi.org/10.6084/m9.figshare.32652846. g. Molecular formula of the respective product of each reaction shown in (f).

| Time [min] | A [%] | B [%] | Flow [mL/min] |
|---|---|---|---|
| **0.00** | 70. | 30 | 0.4 |
| **1.00** | 70 | 30 | 0.4 |
| **8.00** | 2 | 98 | 0.4 |
| **9.50** | 2 | 98 | 0.4 |
| **9.60** | 70 | 30 | 0.4 |
| **10.00** | 70 | 30 | 0.4 |

**Figure S12**: **Gradient steps for 30% acetonitrile LC-Method used for myriocin detection**.

A = MeCN. B = $H_2O$ + 0.1% formic acid.

a

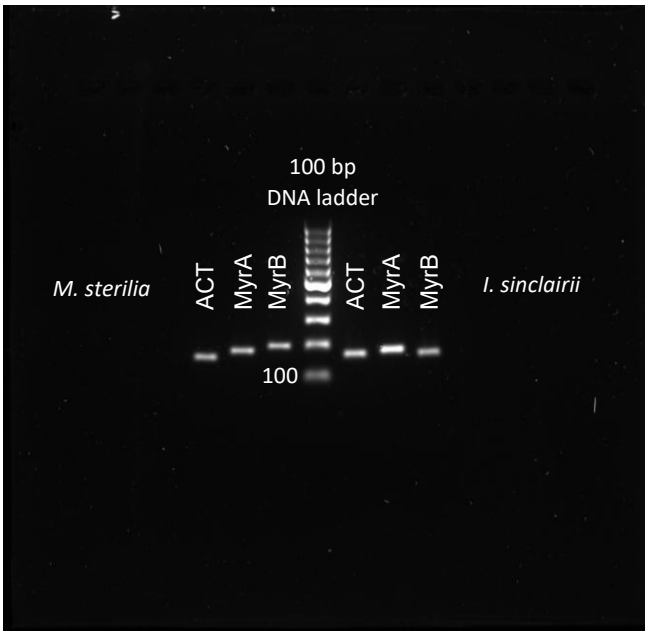


b

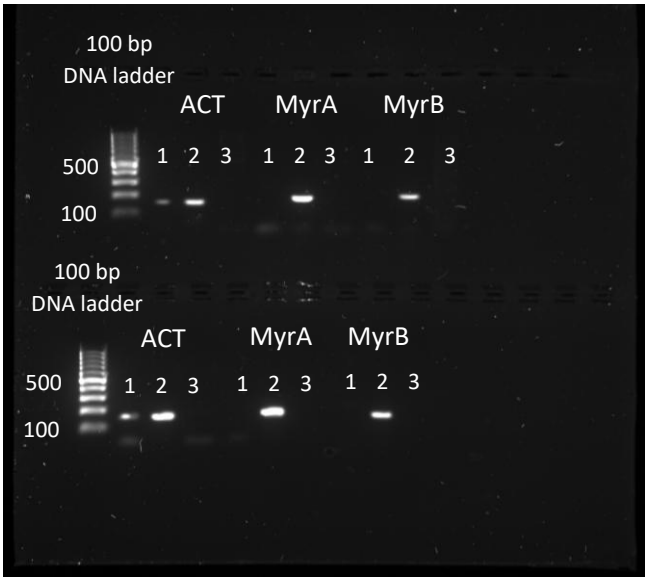


**Fig. S13: Uncropped gel images of PCR and RT-PCR products shown in Fig. 4.** a. PCR products from genomic DNA for actin *myrA* and *myrB*. Left: *M. sterilia*, right: *I. sinclairii.*
b. RT-PCR products for actin, *myrA* and *myrB* (1 = Day 10, 2 = Day 20, 3 = No nucleic acid control). Above: *M. sterilia*, below: *I. sinclairii.*

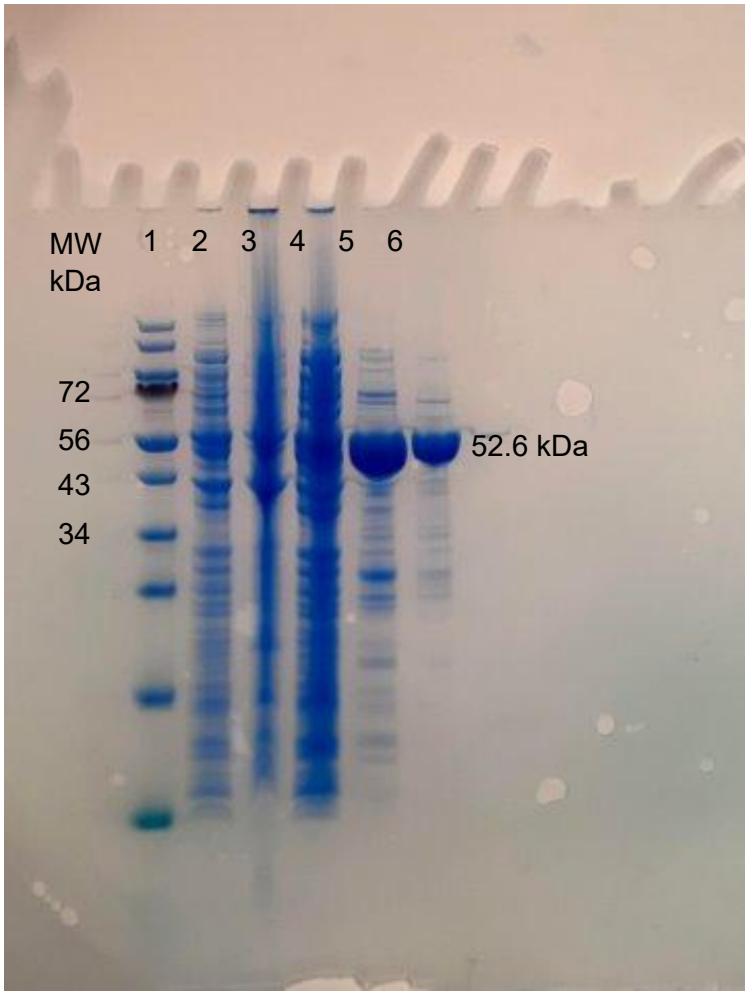


**Fig. S14: Uncropped SDS-PAGE gel images of purified recombinant IsMyrA shown in Fig. 6 and Fig. S11.**
Lanes (from left to right): 1. Protein molecular weight ladder (kDa); 2. Total lysate; 3. Pellet; 4. Supernatant; 5. IsAOS after Histrap; 6. IsAOS after SEC.